Unsteady Computational Study of Novel Biologically Inspired Offshore Vertical Axis Wind Turbine at Different Tip Speed Ratios: A Two-Dimensional Study

S. N. Ashwindran, A. A. Azizuddin* and A. N. Oumer

Faculty of Mechanical Engineering, Universiti Malaysia Pahang, 26600 Pekan Pahang, Malaysia
*Email: azizuddin@ump.edu.my
Phone: +6094246231; Fax: +6094246222

ABSTRACT

The aim of this paper presents an unsteady numerical investigation of a novel biologically inspired vertical axis wind turbine for offshore regions of Malaysia. The proposed blade shape is a result of hybrid design inspired by maple seed and epilobium hirsutum. The simulation was conducted in 2D using the sliding mesh technique with non-conformal mesh spatial discretisation via FLUENT 16.2. A grid sensitivity study on mesh density and turbulent transport model indicated that fine mesh and medium converged well with trivial difference. SST and k-ω model presented stable behaviour and indicated good agreement. The proposed wind turbine was simulated at five different moderate tip speed ratios under the influence of freestream velocity U_∞=8 m/s. The highest moment coefficient is generated at tip speed ratio λ=1.3, which is C_m=0.1886 with a stable positive moment coefficient after 480°. The proposed turbine responded well at λ=1.3 and λ=1.7 with power coefficient result of C_p=0.245 and C_p=0.262 respectively. The effect of wake and vorticity on the turbine at subjected tip speed ratios is studied. Wake regions induced by the leading edge of the aerofoil impacted the performance of the following blade. Due to the less wake effect trailed by the leading edge at λ=1.3, it generates higher moment than λ=1.7.

Keywords: Vertical axis wind turbine; CFD; biomimicry; wind energy; sliding mesh.

INTRODUCTION

In the world of a rapidly growing economy, energy consumption by industry and domestic are drastically rising, which is leading to an energy crisis. Today many countries are investing their resources on the development of renewable energy; with notable development in wind power generation. It is the oldest form of harnessing energy by extracting kinetic energy of moving air and converting it to mechanical energy. Installation of wind turbine type and size of a wind turbine are dependent on wind speed potential and geographical area. Wind energy harvesting can be classified into two categories, which is offshore and onshore. Research shows that offshore wind energy harvesting is regarded as a clean energy source due to its minimal environment effect and has the lowest green-house gas (GHG) emission in comparison to other renewable energy counterparts [1]. Relevant studies on GHG lifecycle and environmental impact pertaining to wind power technologies can be found in [2–6].

In recent years the ministry of energy, green technology and water (KeTTHA), have adapted the five-fuel diversification strategy energy mix which comprises of nature gas, coal, oil, hydropower and renewable energy [7]. In Malaysia, the research and

development in wind power harvesting started in the early 1990s, where research and studies being conducted unable to convince and show the potential of wind energy. The reason was due to lack of political support and poor methodologies and instrumentation, resulting in inaccurate and unreliable wind potential data [8]. Sustainable Energy Development Authority (SEDA) was formed in 2011 to manage funds allocated for renewable energy development implemented in Feed-in tariff (Fit) under the Renewable Energy Act 2011. Although there are no feed-in tariffs for wind energy, with Malaysia geographical area provides a great platform for ocean-based energy harvesting, especially with strong winds from northeast and southwest from the Indian ocean [9]. Case in point, Tenaga National Berhad (TNB) was the first to adapt wind energy harvesting with 200kW power capacity and able to supply enough electricity approximately for 200 households in the regions of Perhentian island [10].

Studies show that Malaysia coastline extends to 4675km, which is the 29th longest coastline [11]. Research done in Malaysia was mainly focused on onshore and costal wind. However, no study was done on Voluntary Observation Ship (VOS) offshore data due to insufficient data reports. Therefore, it is difficult to estimate the wind speed potential accurately [8]. Wind speed in Malaysia is dominated by seasons; northeast monsoon season; southwest monsoon season. Northeast monsoon occurs from November to March; southeast monsoon season starts from June to September. Northeast monsoon mainly experiences rainy season due to cold air from Siberia. Studies show that during monsoon season, mean wind speed potential reaches up to 15m/s for East Coast regions [12]. The wind speed can reach up to 10m/s in the offshore points of Sabah and Sarawak due to the impact of typhoon occurring in the neighbouring countries such as the Philippines [13].

Research shows that offshore wind technology facilities are developing at a rapid rate in comparison to onshore wind turbine installation and other renewable energy resources [14–17]. Offshore wind facilities hold advantage over onshore facilities due to; offshore wind facilities produce fewer greenhouse gases than onshore wind turbines by 48% per kWh [18]; offshore load centres are more practical then onshore where the public grid is not effective for interstate power transmission; offshore winds are more steady, strong, stable, higher energy with minimal shear and less turbulent than onshore wind; vast construction site for offshore wind facilities than limited land area for onshore. Potential on offshore wind power harvesting can be found in [19–21].

The present work aims to investigate the power extraction performance of the proposed biologically inspired wind turbine for harvesting wind energy in offshore regions of Malaysia. Due to the inconsistent seasonal wind speed potential in the regions of Malaysia. Thus, new technologies and blade configuration have to be implemented to adapt to wind behaviour in the regions of Malaysia. Hence this paper presents the computational numerical investigation of the proposed design at moderate tip speed ratio to understand the behaviour and flow properties relative to offshore wind speed potential of Malaysia. Offshore wind energy harvesting constitutes greater potential than onshore wind turbines due to its moderate wind speed during the non-monsoon season and high wind speed in monsoon seasons.

Biologically Inspired Designs in Wind Turbine Applications

Fish et al.[22] researched the tubercles of humpback whale's flippers. The author stated that the motion of the flippers was improved by passive flow control mechanism contributed by tubercles. The authors carried out an analysis of the wing model integrated

with tubercles. The result shows tubercles had increased the lift value and consequently decreased the drag value. Cognet et al. [23] reported a novel elastic wind turbine blade inspired by insect flight and plant reconfiguration. The elastic blade works on the principal of blade deformation due to air loading and centrifugal effects. The authors stated that the bio-inspired design contributed to the improvement of efficiency of the turbine up to 35% in comparison to conventional rigid blade design. Lentink [24] researched the aerodynamic performance of auto-rotating plants seeds. The author carried out research on modelled three-dimension maple and hornbeam seeds to study its morphology and kinematics. Study shows that maple seeds morphological properties made it be dispersed in high wind conditions. At low wind velocity, auto-rotating seeds can generate high lift force regardless of its small size. The mechanism that contributes to high lift force generation as it descends is the leading-edge vortex (LEV). LEV mechanism is not only found in auto-rotating plants, birds and insects also analyse this mechanism to glide and hover. Minami et al. [25] conducted a study on the aerodynamic and flight dynamics of pappose and winged seeds. The author stated that there are four flying modes in seeds, which are parachuting, gliding, rocking and spinning. The flight motion of winged seeds depends on their centre of gravity. Winged seeds analyse a gliding angle for motion, lift and moment generation. More information on biologically inspired wind turbine research can be found in [26–30].

Past CFD Numerical Analysis

Elkhoury et al. [31] carried out wind tunnel experiment and numerical simulation on a Qrthopther-type vertical axis wind turbine. In the unsteady computational setup, Delayed Detached Eddy (DDES) using the Spalart-Allmaras (SA) turbulent model was used to simulate the 3D model in ANSYS 16.2. The result showed that the power coefficient increases with increasing velocity. Furthermore, at the lowest aspect ratio of 1.0 and highest solidity of 0.75, the power coefficient was found to be at its maximum. Marten et al. [32] investigated on non-linear lifting line free vortex wake algorithm implemented in Q-blade wind turbine simulation code. The result showed that, under tower blockage, the implemented code provides a time accurate simulation in turbulent wind fields. The result came in good agreement when validated against several other codes and experimental result.

Li et al. [33] studied the application of blade pitch control on VAWT. Five governing equations were used to analyse the relationship between blade pitch control and the generated output. The unsteady CFD analysis was performed in 2D, and the result was validated with wind tunnel experiment. The results showed that the optimised blade pitch in two vertical axis wind turbines (VAWTs) with different chord length increases with an average power coefficient of 0.177 and 0.317, respectively. Subramanian et al. [34] studied the effects of the performance of VAWT caused by solidity and air profile. Ansys FLUENT was used to study 1.1kW Darrieus VAWT. In the study, four different aerofoils were considered-NACA 0012, NACA 0015, NACA 0030, and AIR 001. The result showed that with an incoming velocity of 10 m/s, tip speed ratio varied from 1 to 2.5. Furthermore, the result showed that at low tip speed ratio NACA 0030 has better performance. For tip speed ratio greater than 1.8, NACA 0012 resulted in better performance. Moreover, shear stress transport (SST) is more suitable to analyse a small-scale wind turbine. Lee et al. [35] studied the performance of Darrieus type VAWT using NACA 0015. The authors stated that the parameters such as chord length, helical length, pitch angle and rotor diameter influence the performance of VAWT. In the CFD

numerical analysis, unsteady Reynolds averaged Navier Stokes equation (URANS) with sliding mesh technique was used to analyse the rotational effect of the blades.

Tahani et al. [36] proposed Savonius wind turbine design integrated with direct discharge flow capabilities for building ventilation. The 3D model of the wind turbine is simulated using SST k-ω. The author evaluated four turbulent models to find a suitable turbulent for the analysis, which is k-ω, k-ε, SST and renormalised group (RNG) k-ε. It is found that SST k-ω provides a better result than other turbulent transport models. M. S. Hameed [37] studied on small-scale vertical axis wind turbine aiming 1kW power output for domestic use. Static 3D model at a selected pitch angle was simulated in Ansys 13.0. The software generated result was evaluated with the analytical result at a similar location. The percentage of error was 9.46 % when drag value of CFD and the analytical result was compared. The numerical error can be further reduced by improving the grid resolution. Based on the literature review, ANSYS commercial software is widely used by researchers in conducting a numerical investigation on wind turbines due to its robust CFD packages. Furthermore, the numerical model such as URANS and two equation turbulent transport model are accustomed to wind turbine research due to its economic computational load. Hence, URANS model and two equation turbulent transport model is analysed for the investigation of the proposed wind turbine.

COMPUTATIONAL METHODOLOGY

Model Geometry Configuration

Airborne or wind-dispersed seed plants has a unique aerodynamic property for gliding mechanism by rotating on its axis induced by wind flow. The plants disperse or propagate seeds by dispersal vector mechanism; which is dispersing seeds to another location from local point to spread the population. Dispersal vector is classified into two types; active and passive dispersal vector. Wind propagation is a passive disperse vector, which analyses wind kinetic energy for movement. In this research, maple and epilobium hirsutum seed morphology is adapted to model the proposed design. The proposed design was prepared in CATIA V5 using surface morphing technique. The proposed design, as displayed in Figure 1(a), is a lift driven wind turbine consisting of four blades constructed using (national renewable energy laboratory) NREL S819 aerofoil. Case in point NREL is responsible for analysing and classifying aerofoil according to configuration type and aerofoil family. The constructed blade has an angle of twist of 4° facing upwind. The constructed design was prepared using vertical axis configuration design parameters, as illustrated in Eq. (1)-(4). The design parameters such as swept area (S_A), aspect ratio (A.R), height (H), and rotor diameter (D_r), are reported in Table 1 and Figure 1(c). Since the simulation conducted in 2D, the height ($H_{simulation}$), is set to 1m due to ANSYS FLUENT default setting for 2D numerical study. As illustrated in Figure 1(b) the adapted morphology is segmented into two parts; the upper and lower segment. The lower segment is morphology is inspired by maple seed, and the upper segment is adapted from epilobium hirsutum. In this research, the effect of the constructed morphology on the aerodynamic performance was analysed in 2D relative to the aerofoil type chosen; NREL S819. A planar section of the turbine at 0.8m from datum labelled as 'C' as displayed in Figure 1(c) were selected to be simulated as it is the critical region in the proposed wind turbine. The model is simulated in 2D to save computational power and numerical analysis time. Table 2 report the design parameters.

$$A.R = \frac{H}{D_r} \tag{1}$$

$$S_{A-Actual} = D_r \times H \tag{2}$$

$$S_{A-simulation} = D_r \times H_{simulation} \tag{3}$$

$$\sigma = \frac{B \times c}{\pi \times D_r} \tag{4}$$

Table 1. Rotor blade properties.

Rotor	Chord, C (mm)	Thickness, t (mm)	Solidity, σ
NREL S819	310	56	0.25

Table 2. Design parameters.

Design parameters	Symbol	Dimension
Number of blades	B	4
Swept area	S_A (mm)	2.93m^2
Rotor diameter	D_r (mm)	1.6m
height	H (mm)	1.33m
Aspect ratio	A.R	0.83
Angle of attack	AoA	4°

(a)　　　　　　　　(b)

(c)
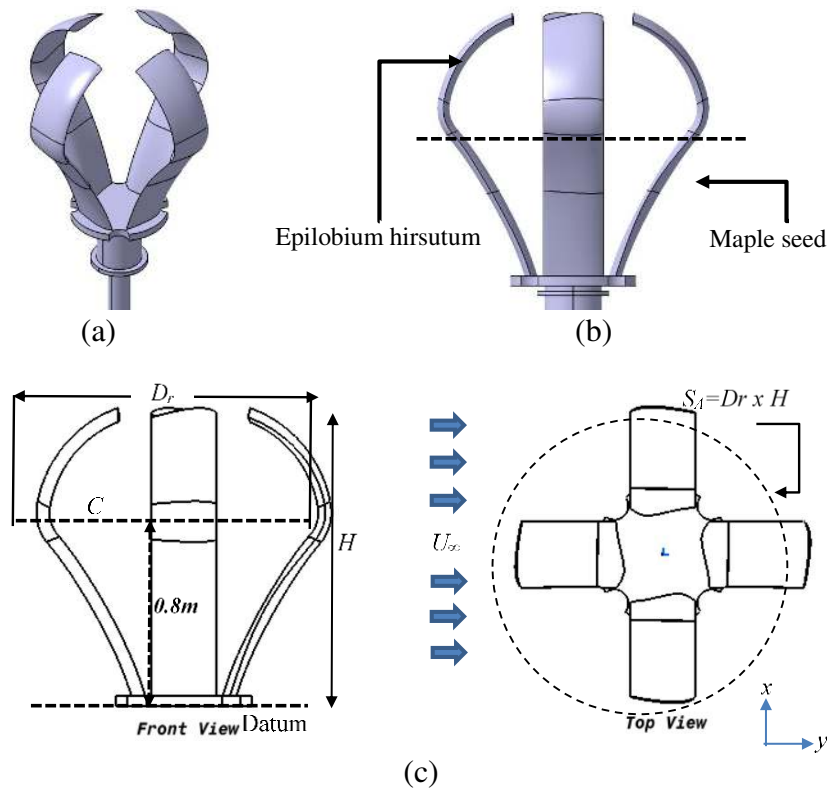
Figure 1. Proposed wind turbine configuration: (a) wind turbine design, (b) adapted morphology, (c) wind turbine configuration.

(a)

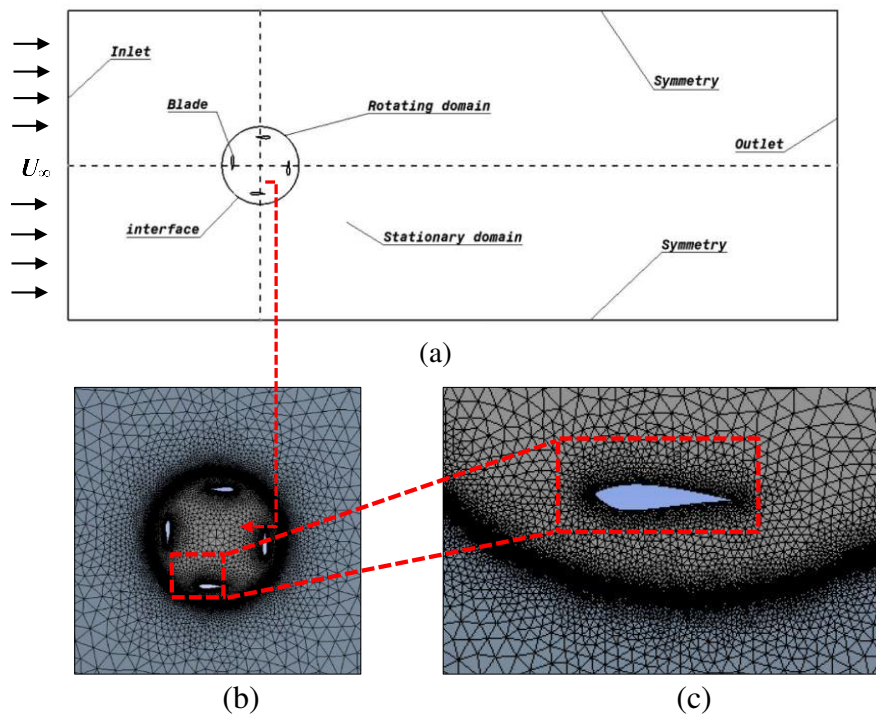(b)   (c)

Figure 2. Proposed wind turbine configuration: (a) Proposed wind turbine design, (b) adapted morphology.

Domain and Mesh Topology Configuration

Proper domain modelling and space discretisation in a CFD analysis have an impact on flow field response, where factors influencing the flow field are based on the parameters initialised at the domain. Furthermore, defined boundary condition and domain dimension dictate the influencing parameter in an unsteady flow field such as turbulent intensity, hydraulic diameter, turbulent viscosity ratio, etc. As illustrated in Figure 2(a), the virtual wind tunnel domain consists of two domains; main domain and rotating domain. The main is composed of an inlet, two symmetry boundaries, and an outlet. Since sliding mesh technique via the finite volume method (FVM) were used in this research, the rotating domain is separated from the main domain to ensure non-connectivity within the nodes of the domains. More information on FVM can be found in [38–41]. Furthermore, the sliding mesh method (SMM) is widely used in a research study related to rotating machinery [42]. The main domain dimension is constructed relative to rotor diameter, D_r. As illustrated in Figure 2(a), the free stream wind flows from the inlet boundary from left to right. In this research, non-conformal mesh method was used to discretise the spatial domain. The main domain was discretised as static mesh and the rotating domain as moving mesh separated by an interface. As displayed in Figure 2(b), 2(c), the domains were discretised under different mesh parameters to ensure minimal computational cost and different mesh densities between the domains. The domains were composed of the unstructured triangular mesh. Four different size function were employed on the domain; different body size function on main and rotating domains; edge size along the blade regions and on the interface that separates the domains. The generated mesh topology indicates good mesh metric results. The mesh topology is prepared under fine and medium mesh resolution for mesh dependency study. Table 3 report the mesh parameters.

Table 3. Mesh parameters.

Mesh resolution	Medium Mesh	Fine mesh
Number of elements	84890	157976
Simulation time	2 hour and 17 min	6 hours and 32 min

Turbulent Modelling

In this numerical study, unsteady Reynolds averaged Navier-Stokes equation (URANS) were used to study the complex flow field. URANS numerical model was chosen because of its robustness in analysing wind turbine and minimal computational cost. URANS model work on the principle of computing Navier Stokes equation by numerical decomposition or also known as Reynolds decomposition, as stated in Eq. (7). Reynolds decomposition is the sum of fluctuating and mean components by time average [43]. URANS model was developed to compute Reynolds stress in a fluid flow. In this numerical study, Reynolds stress is computed by linear eddy viscosity approach using two equation turbulent transport model. To study the reliability of the models, three turbulent transport models were considered; k-ε, k-ω, and SST. The discrepancy of the three models was studied to find the suitable turbulent transport model for analysing the proposed wind turbine with less computational time and reliable result. Since the simulations were conducted in 2D, the governing equations are simplified to x and y components, as shown in Eq. (10)-(12). As displayed in Eq. (5), the flow regime can be enumerated using Reynolds formulation; Where U_∞ is free to stream velocity, x represents the physical length, and μ as dynamic viscosity. In this research, the Eq. 5 is modified to suit the case study, as illustrated in Eq. (6). Therefore, the Reynolds number is 8.66×10^5.

The two-equation turbulent transport model is the most commonly used turbulent model in wind turbine CFD analysis. Two-equation turbulent transport can be classified into two major groups, k-ε and k-ω models. Wolfe [44] stated that the k-ε model is the most suitable to analyse flow field separation for HAWTs. Menter [45] investigated two versions of the k-ω turbulent transport model: baseline (BSL) model and shear stress model (SST). The author stated that BSL model was intended to generate numerical result as k-ω of Wilcox, but the results changes to standard k-ε in k-ω formulation when approaching boundary layer edge. However, the results are similar to Wilcox model within 50% of the boundary layer. In the SST model principal shear stress is proportional to turbulent kinetic energy based on Bradshaw's assumption. The author concluded that the result on adverse pressure gradient using the SST model provides a better agreement with experimental result in comparison to BSL model. Ntinas et al. [46] stated that the standard k-ω model is more suitable for high turbulent airflow cases because of its sensitivity to near wall distribution. SST models are proven to generate highly accurate results concerning to airflow study, because of its collaborating features of standard k-ε and standard k-ω. Ramponi et al. [47] stated that the SST model outperformed other turbulent transport models concerning the respective research and often preferred by researchers. Information on turbulent transport model can be found in [48].

$$Re = \frac{\rho U_\infty x}{\mu} \tag{5}$$

$$Re = \frac{\rho U_\infty D_r}{\mu} \tag{6}$$

Reynolds decomposition

$$u(x,y,z,t) = \overline{u}(x,y,z) + u'(x,y,z,t) \tag{7}$$

Turbulent kinetic energy k-equation

$$\frac{\partial k}{\partial t} + U_j \frac{\partial k}{\partial x_j} = P_k - \beta^* k\omega + \frac{\partial}{\partial x_j}\left[(v + \sigma_k \nu_T)\frac{\partial k}{\partial x_j}\right] \tag{8}$$

Specific rate of dissipation of kinetic energy, ω- equation

$$\frac{\partial \omega}{\partial t} + U_j \frac{\partial \omega}{\partial x_j} = aS^2 - \beta\omega^2 + \frac{\partial}{\partial x_j}\left[(\nu + \sigma_\omega \nu_T)\frac{\partial \omega}{\partial x_j}\right] + 2(1 - F_1)\sigma_{\omega^2}\frac{1}{\omega}\frac{\partial k}{\partial x_i}\frac{\partial \omega}{\partial x_i} \tag{9}$$

Continuity equation,

$$\frac{d}{dt}\int_{cv} \rho\nu + \int_{cs} \upsilon \bullet n\rho dA = 0 \tag{10}$$

Momentum equation,

$$u\frac{\partial u}{\partial x} + \upsilon\frac{\partial u}{\partial y} = -\frac{1}{\rho}\frac{\partial \rho}{\partial x} \tag{11}$$

$$u\frac{\partial \upsilon}{\partial x} + \upsilon\frac{\partial \upsilon}{\partial y} = -\frac{1}{\rho}\frac{\partial \rho}{\partial y} \tag{12}$$

Boundary condition

In this study, the boundary condition was defined in a specific direction to analyse the credibility of the proposed shape morphology. The inlet freestream velocity is constant U_∞=8m/s in the x-direction from left to right. The outlet gauge pressure was set to 0 pascal. The bounding surrounding walls top and bottom were set to symmetry with free slip condition. Hence this would avoid a solid blockage effect [49, 50]. Interfaces around the circular rotating domain were separated into the static and rotating domain. The rotating domain is positioned further from the outlet, as displayed in Figure 2(a) is to avoid backflow or reverse flow. Since sliding mesh technique was used, the rotating domain was set to multiple RPM values under constant inlet freestream velocity in order to numerate the power coefficient (C_p) at different tip speed ratio (TSR). The blade walls were set to no-slip condition and rotation motion relative to the rotating domain cell zone. The rotating domain axis (x; y) were set to (0; 0) under specific RPM values of; 100, 150, 200, 250, and 300. In order to minimise computational power and to avoid numerical errors, the turbulent parameters such as turbulent intensity (I) and turbulent viscosity (μ_t/μ) were maintained to default values. Table 4 reports the boundary conditions parameters.

Table 4. Boundary condition parameters.

Boundary conditions	Parameters	Values
Inlet	U_∞	Constant 8m/s
Outlet pressure	-	0-pascal
Walls	Symmetry	-
Blade walls	No slip condition	-
Angular velocity (*RPM*)	ω	100, 150, 200, 250, 300
Turbulent intensity	I	5%
Turbulent viscosity	μ_t/μ	10

Solver Configuration

The proposed 2D model is simulated under transient (unsteady) configuration. In this transient simulation, Pressure-based solver with absolute velocity formulation was used by stipulating incompressible flow. In order to study the numerical behaviour relative to the proposed model, three types of turbulent transport model were studied; k-ω; realisable with scalable wall function k-ε; and SST. The turbulent transport model was analysed under a similar solver configuration. In cell zone condition, the rotating zone was set to mesh motion under five different RPM rate under constant inlet velocity. Therefore the time marching discretisation such as time-step size, several iterations was dependent on RPM relative to four complete revolutions. Table 5 report the solver configuration. In the pressure-velocity coupling solution method, COUPLE scheme was used, where turbulent kinetic energy and turbulent dissipation rate were set to second order upwind respectively to all turbulent transport models. Courant number was set at 10, explicit relaxation factor was set 0.7, and under-relaxation factor was set to default to obtain stable numerical solutions.

Meanwhile, in reference value, the reference area was set to 1.6m^2 and length of 0.8m. The residual convergence criteria were set to 10^{-5}. The reference area value is rotor diameter (D_r) multiple to 1m because for 2D simulation in ANSYS the height is set to 1m [51–53]. In terms of time-step size and number of iterations, Eq. (13)-(15) were used to numerate the value for four complete revolutions. The number of iterations per time step was set to 20. Generally, more than three complete revolutions are recommended in analysing a wind turbine to remove the initial boundary conditions caused by the primary revolution.

$$\omega = 2\pi \frac{f}{60} \tag{13}$$

$$\omega = 2\pi f = \theta - \theta_0/dt \tag{14}$$

$$dt = 2\pi/\omega \tag{15}$$

Numerical Performance Parameters

In order to understand the behaviour of the turbine, aerodynamic parameters, as shown in Eq. (16)-(21) are taken into careful consideration. Since the proposed design operates in a fixed angle of attack (AoA), moment and lift coefficient generation under different tip speed ratios were studied to analyse power extraction or power coefficient (C_p) of the

design relative proposed morphology and chosen aerofoil type. As manifested in Betz Limit, the maximum power coefficient limit of a wind turbine regardless of the configuration and design is C_p=0.593 [54]. Therefore, the theoretical limit is being analysed as a benchmark to study the performance of the proposed design in wind energy harvesting. Equation (21) is being used to enumerate the generated power coefficient relative to the moment coefficient and tip speed ratio.

In this unsteady study, a 2D graphical representation of the turbine is being developed to understand the motion of the turbine relative to azimuthal increment for a complete revolution ($0 \leq \theta \leq 360$). As displayed in Figure 3, the circumference is divided into four segments, respectively representing a complete revolution. The segments are upwind; windward; downwind and leeward in a clockwise direction. Similar schematic representation concept is presented by Rezaeiha et al. [55]. The aerofoil behaves distinctly different in each segment due to the dissimilarities in lift generation and flows field properties. The magnitude of generated lift is relative to the AoA, orientation and segment of the aerofoil. Each segment represents an angular position of the wind turbine relative to freestream velocity (U_∞). Upwind is from $45 \leq \theta \leq 135$; leeward is ($135 \leq \theta \leq 225$); downwind is $225 \leq \theta \leq 315$ and windward is $315 \leq \theta \leq 45$.

Table 5. Solver configurations.

Solver configuration	Parameters	Values
Turbulent transport model	SST, k-ε, k-ω	-
Reference value	Reference area	$1.6m^2$
Pressure-velocity coupling scheme	COUPLE	-
Spatial discretisation	Second order upwind	-
Convergence criteria	Residual monitor	10^{-5}
Time step	Size	0.01
Number of complete revolutions	n	4

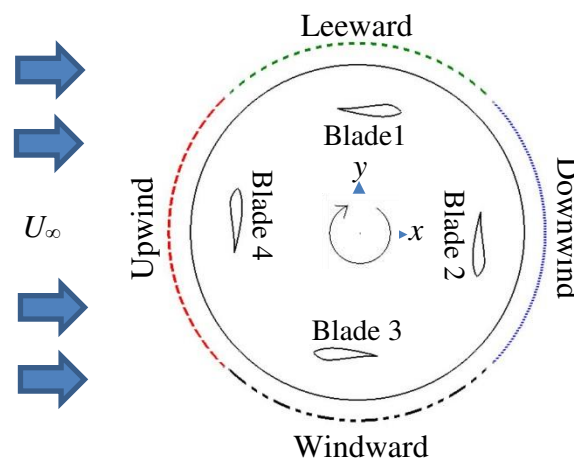Figure 3. Schematic representation of wind direction segments.

Moment coefficient, $C_m = \dfrac{M}{\frac{1}{2}\rho U_\infty^2 D_t}$ $\qquad\qquad$ (16)

Lift coefficient, $C_L = \dfrac{F_L}{\frac{1}{2}\rho S_A U_\infty^2}$ (17)

Tip speed ratio, $\omega = 2\pi f$ (18)

$v = \omega \times \left(\dfrac{D_r}{2}\right)$ (19)

$TSR(\lambda) = \dfrac{\omega \times \left(\dfrac{D_r}{2}\right)}{U_\infty}$ (20)

Power coefficient, $C_p = C_m \times TSR$ (21)

CFD NUMERICAL RESULT

Mesh Densities Sensitivity Study

The proposed design was simulated under different discretised mesh resolution; a fine and medium mesh. The purpose of the mesh dependency study is to find the optimal mesh density for spatial discretisation for minimal computational cost without affecting the accuracy and reliability of the result. The generated aerodynamic response result of the turbine was observed to find the discrepancy under fine and medium mesh resolution. The proposed wind turbine was simulated in 2D under the influence of U_∞= 8m/s free-stream wind speed and tip-speed ratio, (λ) of 1.3, as displayed in Figure 4(a). The presented result indicated trivial dissimilarities between the fine and medium mesh. Both mesh indicates good agreement at a different number of elements, which is 157976 elements for fine mesh and 84890 elements for the medium mesh. Medium mesh consumed less computational time in comparison to fine mesh. The generated total moment coefficient results of the proposed wind turbine indicate good convergence and stable numerical oscillation between two mesh densities. Therefore, fine mesh resolution was chosen because of its more stable and robust numerical solution. As indicated in Figure 4(a), moment generation by the turbine starts to increase and stabilize after 90°, due to the high amount of energy extracted by the turbine blades for motion. As manifested in Figure 4(a) good consistency is observed in upwind region between the mesh densities.

Turbulent Model Sensitivity Study

Three turbulent transport models were chosen for sensitivity study of transport equation relative to discretised spatial resolution. Based on the previous study, a turbulent sensitivity study was simulated at freestream velocity U∞=8m/s, tip-speed ratio (λ)=1.3 under fine mesh density. The chosen turbulent transport model for turbulent sensitivity study was k-ε, k-ω, and SST. As manifested in Figure 4(b), k-ω, and SST has a good agreement in numerical solution with trivial dissimilarities for moment coefficient result for a complete revolution. However, the renormalised group (RNG) k-ε do not agree with SST and k-ω. Major discontinuities generated by RNG k-ε modelling is observed in the upwind region (45<θ<135) in comparison to k-ω, and SST. Based on the generated result, SST model was chosen for the result of the simulations.

In principal SST k-ω is the combination of two formulations; shear stress transport and k-ε. In this hybrid system, it allows SST k-ω formulations to switch behaviour relative to the flow. The researcher in wind turbine simulation widely prefers SST models because of its behaviour pattern in adverse pressure regions. k-ω is a two-equation model, consisting of two extra turbulent equations representing turbulent properties to solve the flow variables. In freestream flow, the k-ω model tends to exhibit issues due to its high sensitivity to turbulent properties and wall functions. Therefore, SST formulations switch modelling behaviour to the k-ε formulation. SST k-ω model is almost similar to the standard k-ω model, but with refined formulation to ensure accuracy and robustness. The combination of SST and k-ω model is called blending function, where the coefficient and cross-diffusion terms in the k-ω equation are altered by SST formulation to ensure appropriate behaviour are exhibited by the model in the far-field zone and near wall region. For simplicity, SST is an auxiliary numerical system for the k-ω model to ensure stability and accuracy in predicting flow field properties. Furthermore, based on the literature survey, SST k-ω model is widely preferred by the researcher in conducting flow field study using the finite volume method (FVM).
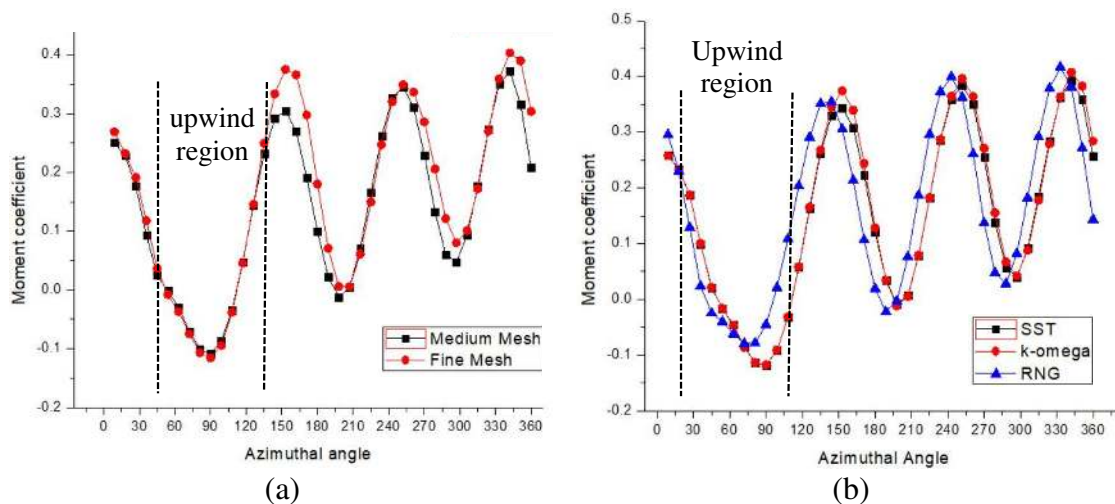

Figure 4. Total moment coefficient vs. azimuthal angle from (a) grid independency test and; (b) turbulent transport model sensitivity study.

RESULTS AND DISCUSSION

The unsteady simulation was conducted using a sliding mesh technique under a non-conformal mesh configuration. Due to the limitation of computational power, the simulation study is conducted in 2D. Only the critical section of the design is analysed to save computational and analysis time. Therefore, the study is conducted by stages to examine the proposed morphology credibility with manifested wind speed potential in offshore regions of Malaysia. This study aims to analyse the generated power coefficients (C_p) over a range of tip speed ratio (TSR) to find the optimum TSR value relative to a wind speed of 8m/s and chosen aerofoil type. The proposed design is comprised of aerofoil type NREL S819 twisted to a fixed AoA of 4°. Based on previous mesh and turbulent model sensitivity study, the simulations were conducted under fine mesh densities and SST turbulent transport model. The 2D turbine is simulated under a range of tip speed ratios, which are 0.85, 1.3, 1.7, 2.1 and 2.6. Due to the complexity of flow regimes properties, this research focusses on the generated result properties in wake

region and power coefficients at subjected tip speed ratio. Figure 5 shows the moment coefficient result at different tip speed ratio. As manifested in the result, the generated oscillating numerical value responded differently at respective tip speed ratio from $90 \leq \theta \leq 360$. It is observed that the highest peak value of moment coefficients is indicated by $\lambda=1.3$ and $\lambda=1.7$ tip speed ratio.

Meanwhile, the lowest moment coefficient result is generated by $\lambda=0.85$. Numerical instability is presented by $\lambda=2.1$ and $\lambda=2.6$ with decreasing moment values. Based on the result, two stable and high moment generating tip speed ratio was chosen for further study, which is $\lambda=1.3$ and $\lambda=1.7$.
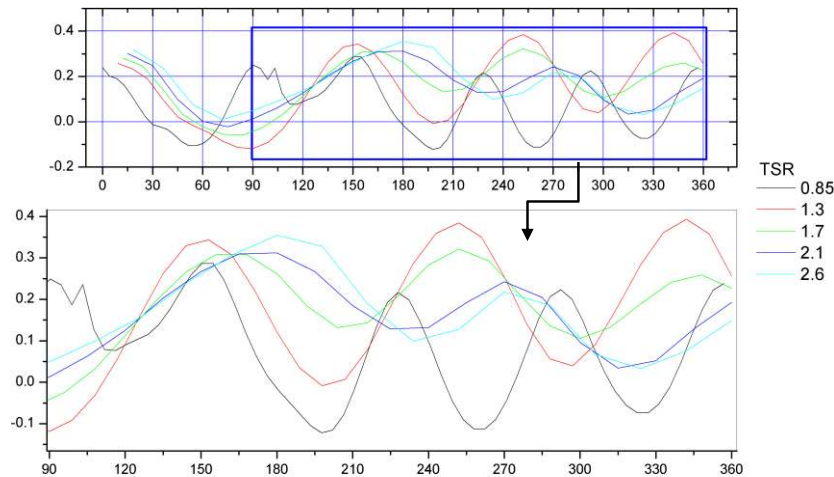
Figure 5. Total moment coefficient against azimuthal angle at different tip speed ratio.

Figure 6 presents the total moment coefficient result vs. azimuthal angle ($0 \leq \theta \leq 1440$) for four complete revolutions at $\lambda=1.3$. The numerical oscillation stabilises after $480°$ with an average stable peak value of $C_m =0.32$. The average of total moment coefficient is $C_m=0.1886$. The turbine generates a stable positive moment coefficient after $480°$. In the first revolution ($0 \leq \theta \leq 360$), numerical instability is observed fluctuating from the steep negative and positive moment. The maximum value of the total moment generated is at $360°$ in the windward segment. The negative moment generated reaches the lowest value at $90°$ as the lift coefficient decreases in the upwind segment, as displayed in Figure 7. After $120°$ moment generation increases to positive values assisted by increasing lift coefficient. Similar generated numerical instability from $0 \leq \theta \leq 360$ can be observed in research presented by Qin et al. [56]. The instability is due to the turbine adjusting its configuration to forces incurred by the flowing wind on the fixed AoA aerofoil geometry. The aerofoil of the proposed design is not a variable pitching blade that changes its aerofoil orientation or AoA to generate optimal lift force. Therefore, it is sensible for the fixed AoA aerofoil for the proposed design to struggle at the initial stage while gaining momentum for a complete revolution. As the revolution progresses, the turbine gains stability and inertia for a stable and positive moment periodic oscillation.

The proposed turbine is defined to rotate at the clockwise direction, and the blades are orientated as displayed in Figure 3. As shown in Figure 8 and Figure 9, blade 3 generated the highest moment and lift result, respectively, at the initial cycle in comparison to other blades. This is because blade 1 aerofoil is facing the windward direction. As the wind flows over the aerofoil, the rate of change of momentum of moving air generates higher lift force in comparison to other aerofoil surface facing in a different

direction. As the flowing wind hits the leading edge and flows over the surface to the leading edge of blade 3 with AoA of 4° the mass of air accelerates faster on the upper surface of blade 3. Therefore, it creates a pressure difference between the upper and lower surface of blade 3, thus generating an upward lift force perpendicular to wind direction.
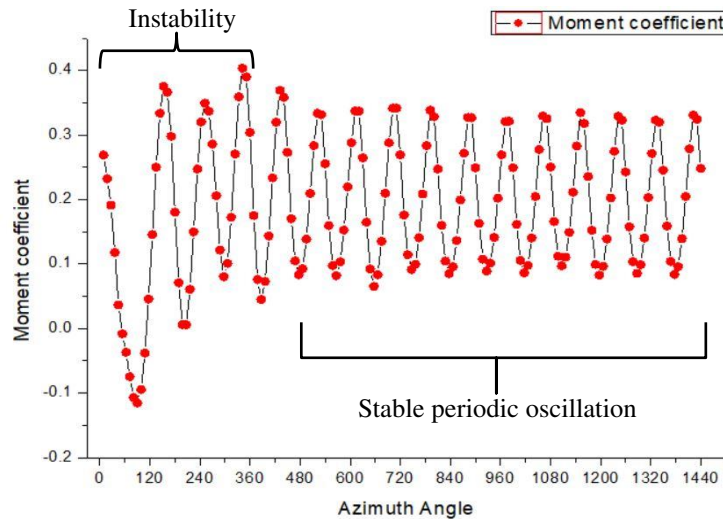

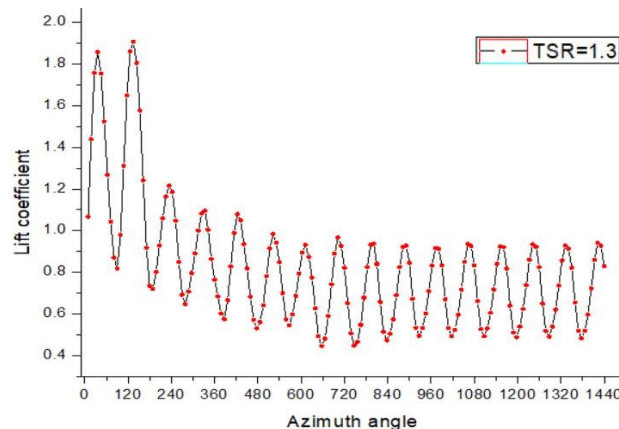Figure 6. Total moment coefficient vs. azimuthal angle for four complete revolutions at λ=1.3.

Figure 7. Total lift coefficient vs azimuthal angle.

Furthermore, as blade 3 moves towards the upwind direction, the magnitude of generated lift increases until it reaches an optimal point. Then the lift force decreases as blade 3 enters the upwind segment. Blade 2 reaches its lowest point in the upwind segment is when the blade is facing normal to the wind direction. As the angular position of the aerofoil of blade 3 progress, the lift component increases in small amount as a result of small incremental in the moment. This is because the blade 3 is still in the upwind region. When blade 1 is in the leeward segment, the aerofoil is orientated in the direction of the flowing wind. Blade 1 is in the opposite orientation to blade 3. Therefore, the flowing wind over the surface of aerofoil of blade 1 generated a downward lift force component. The difference in magnitude of lift components generated by blade 1 and blade 3 is the reason for rotation when subjected to wind at a fixed angle. This behaviour applies to blade 2 and blade 4. The coupling behaviour presented by opposing blades is

governed by Newton's third law. The dissimilar magnitude of opposite forces induced by wind load dictates the direction and magnitude of angular rotation. In this case, blade 3 in windward direction generates higher lift than blade; therefore, rotating in a clockwise direction.
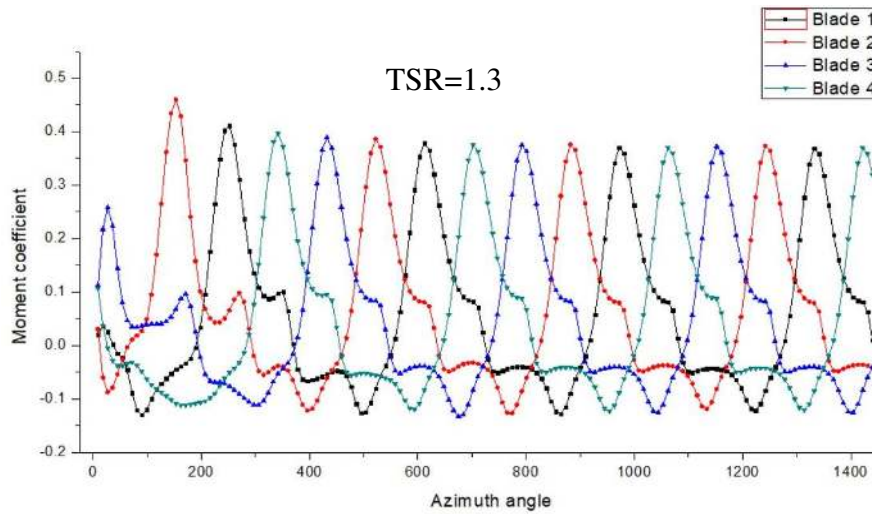

Figure 8. Moment coefficient of blade 1 to 4 responding to azimuthal angle.
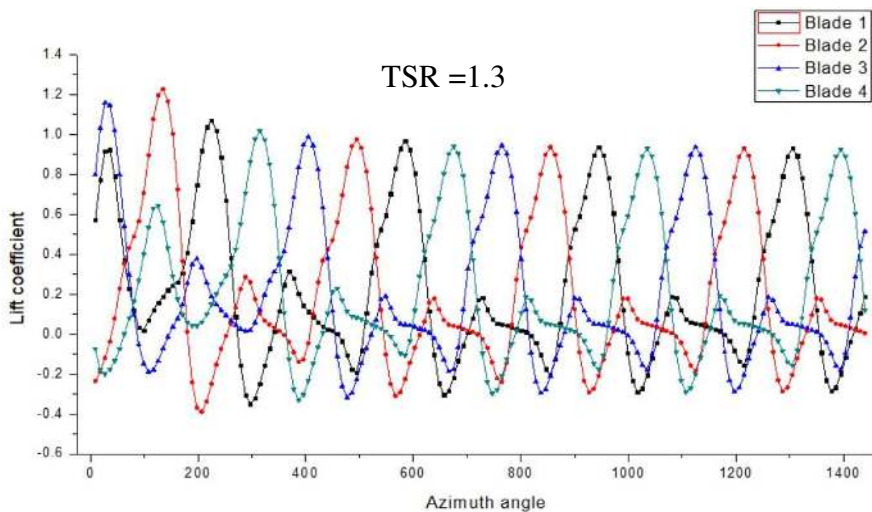

Figure 9. Lift coefficient of blade 1 to 4 responding to azimuthal angle.

Figure 10 presents the result of the total moment coefficient against flow time at $\lambda=1.7$. The turbine generates an average moment coefficient value of $C_m=0.153991$ and shows almost similar behaviour pattern as $\lambda=1.3$ in wind energy extraction. Although it is observed that $\lambda=1.7$ generated less moment than $\lambda=1.3$, the difference is trivial of 0.04 C_m. Power coefficients (C_p) extrapolation indicated that $\lambda=1.7$ scores higher than $\lambda=1.3$ due to angular rotation properties, as displayed in Figure 11. Based on Eq. (22), the numerated average C_p value is $C_p=0.245$ for $\lambda=1.3$ and $C_p=0.262$ for $\lambda=1.7$.

Due to the complex flow properties presented by the turbine, the performance or dynamic response of the turbine can be analysed in terms of wake and vorticity properties. In this study, the vorticity magnitude response of turbine of defined TSR (λ) is studied, to analyse the effects of vortex and wake region. Vorticity magnitude represents the pseudovector field that illustrates the local spinning motion of a continuum near a local

represented point. For simplicity, Eq. (22) represents the magnitude of vorticity in a fluid flow which can be defined under custom field functions in FLUENT.

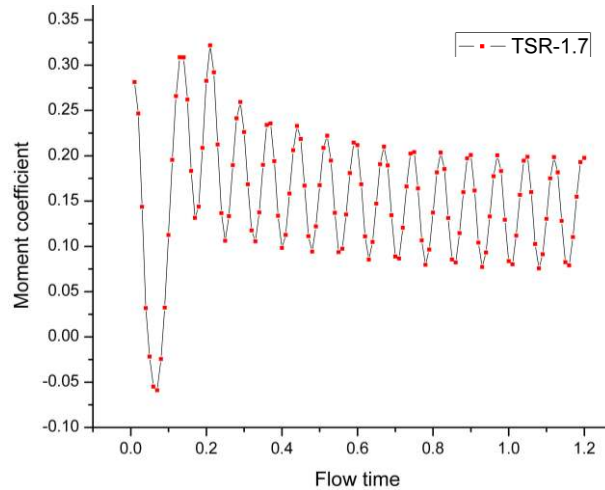$$\frac{dY - velocity}{dx} - \frac{dX - velocity}{dy} \tag{22}$$

Figure 10. Total moment coefficient vs. flow time at λ=1.7.

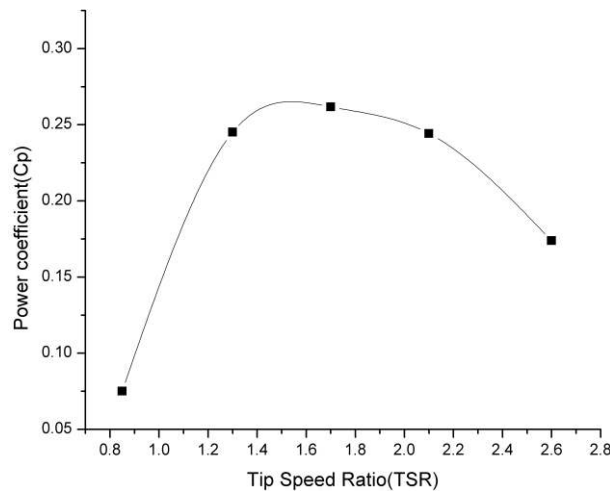Figure 11. Power coefficient vs. tip speed ratio.

Figure 12 represents the vorticity magnitude result under the range from (0-500)*1/s* of the tip speed ratios used in this simulation. As shown in Figure 12(a), blade 1 experienced a strong vortex region or flow circulation on the upper surface of the aerofoil, which affects the lift and moment generation of the aerofoil therefore affecting the performance of the turbine. Meanwhile, in Figure 12(d) and 12(e) strong wake effect is observed on the trailing edge of blade 3 and blade 4, which effects the following blade. Although Figure 12(b) and 12(c) presents almost similar behaviour, the wake intensity of λ=1.3 is weaker than λ=1.7, therefore its sensible for λ=1.3 to generated higher moment and lift magnitude than λ=1.7.

(a) λ=0.85　　　　　　　　　　(b) λ=1.3
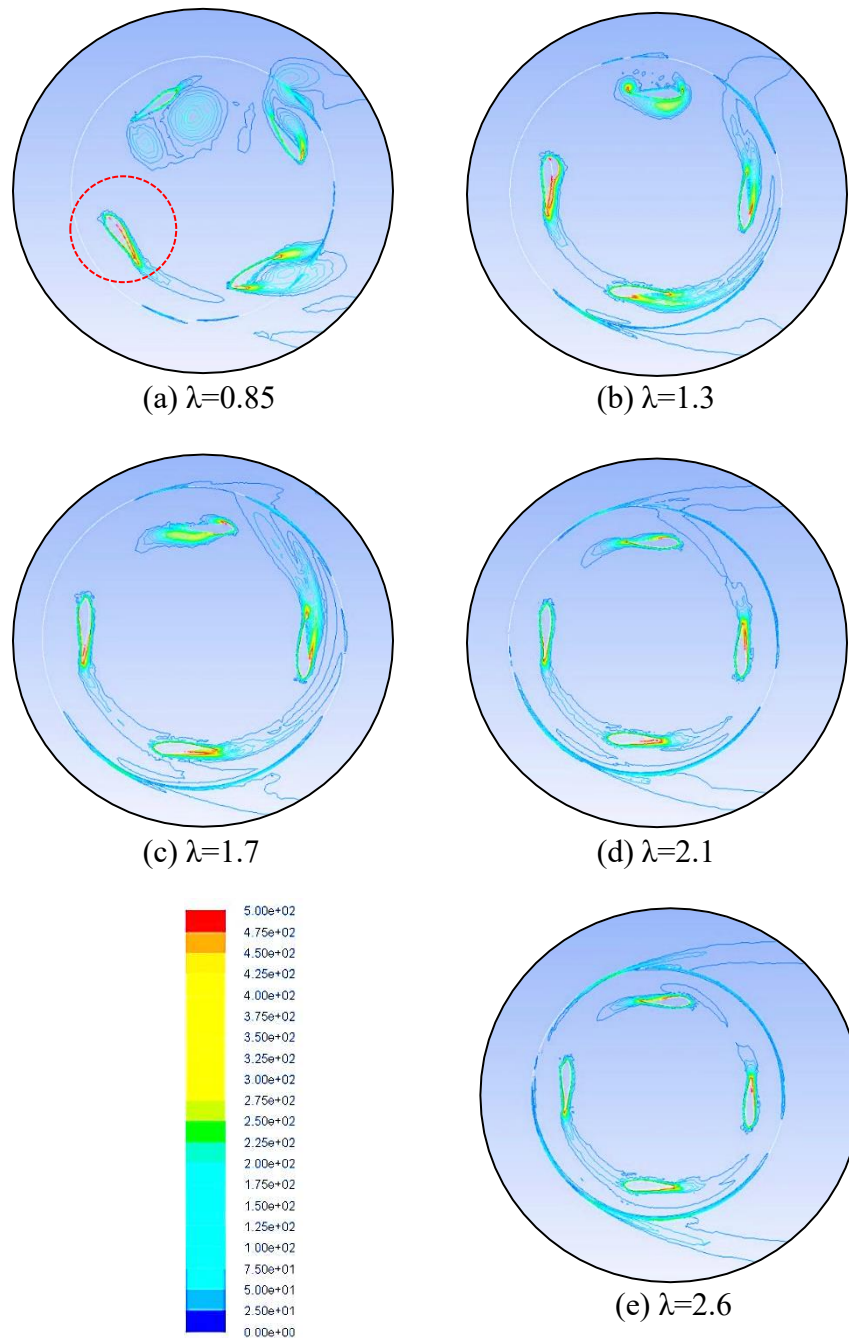
(c) λ=1.7　　　　　　　　　　(d) λ=2.1

(e) λ=2.6

Figure 12. Vorticity magnitude at different tip speed ratio.

CONCLUSION

This paper presents the numerical investigation of a novel bio-inspired vertical axis wind turbine designed for offshore regions of Malaysia. The proposed model was examined at different mesh densities and turbulent model in order to find the proper simulation configuration setting. Five options of tip speed ratio were examined. At tip speed ratio of λ=1.3 the numerical oscillation stabilizes after 480° with an average stable peak value of C_m =0.32. The average of total moment coefficient was C_m=0.1886. Meanwhile, at tip speed ratio λ=1.7 the turbine generated an average moment coefficient value of C_m=0.153991 and showed almost similar behaviour pattern as λ=1.3 in wind energy

extraction. The result showed that the proposed turbine with four blades composed of fixed *AoA* aerofoil NREL S819 performed well at tip speed ratio λ=1.3 and λ=1.7 by generating a stable average power coefficient value of *Cp*=0.245 and *Cp*=0.262 respectively. Furthermore, the vorticity magnitude of each tip speed ratio was analyzed. It was observed that, wake effects induced by the trailing edge had affected the performance of the following blade. It was sensible response to be exhibited by the blade since it was not a variable pitch design. In the future, further investigation is required in order to complete the analysis and understand the aerodynamic behaviour of the proposed morphology blade design and configuration.

ACKNOWLEDGEMENT

REFERENCES

[1] Amponsah NY, Troldborg M, Kington B, et al. Greenhouse gas emissions from renewable energy sources: A review of lifecycle considerations. Renewable and Sustainable Energy Reviews 2014; 39: 461–475.

[2] Hondo H. Life cycle GHG emission analysis of power generation systems: Japanese case. Energy 2005; 30: 2042–2056.

[3] Nomura N, Inaba A, Tonooka Y, et al. Life-cycle emission of oxidic gases from power-generation systems. Applied energy 2001; 68: 215–227.

[4] Tremeac B, Meunier F. Life cycle analysis of 4.5 MW and 250 W wind turbines. Renewable and Sustainable Energy Reviews 2009; 13: 2104–2110.

[5] Martínez E, Sanz F, Pellegrini S, et al. Life cycle assessment of a multi-megawatt wind turbine. Renewable Energy 2009; 34: 667–673.

[6] Wang Y, Sun T. Life cycle assessment of CO 2 emissions from wind power plants: Methodology and case studies. Renewable Energy 2012; 43: 30–36.

[7] Salleh NF, Chew BC, Hamid SR. Feasible application of offshore wind turbines in Labuan Island, Sabah for energy complementary. In: AIP Conference Proceedings. 2017.

[8] Ho L. Wind energy in Malaysia : Past , present and future. Renewable and Sustainable Energy Reviews 2016; 53: 279–295.

[9] Mekhilef S, Safari A, Chandrasegaran D. Feasibility study of off-shore wind farms in Malaysia. Energy Education Science and Technology Part A: Energy Science and Research 2012; 29: 519–530.

[10] Ibrahim HN. Towards renewable energy. Tenaga Link Malaysia 2011; 1: 1–20.

[11] Ahmad S, Tahar RM. Selection of renewable energy sources for sustainable development of electricity generation system using analytic hierarchy process: A case of Malaysia. Renewable Energy 2014; 63: 458–466.

[12] Najid SK, Zaharim A, Razali AM, et al. Analyzing the East Coast Malaysia Wind Speed Data. 3.

[13] Ahmad Zaman AA, Hashim FE, Yaakob O. Satellite-based offshore wind energy resource mapping in Malaysia. Journal of Marine Science and Application 2019; 18: 114–121.

[14] Adedipe O, Abolarin MS, Mamman RO. A review of onshore and offshore wind energy potential in Nigeria. In: IOP Conference Series: Materials Science and

Engineering. 2018.

[15] Chipindula J, Botlaguduru VSV, Du H, et al. Life cycle environmental impact of onshore and offshore wind farms in Texas. Sustainability 2018; 10: 1–18.

[16] Keivanpour S, Ramudhin A, Ait Kadi D. The sustainable worldwide offshore wind energy potential:A systematic review.Journal of Renewable and Sustainable Energy 2017;9: 065902.

[17] Konstantinidis EI, Botsaris PN. Wind turbines: Current status, obstacles, trends and technologies. In: IOP Conference Series: Materials Science and Engineering. 2016.

[18] Noori M, Kucukvar M, Tatari O. Economic input-output based sustainability analysis of onshore and offshore wind energy systems. International Journal of Green Energy 2015; 12: 939–948.

[19] Mekhilef S, Chandrasegaran D. Assessment of off-shore wind farms in Malaysia. In: IEEE Region 10 Annual International Conference, Proceedings/TENCON. IEEE, 2011, pp. 1351–1355.

[20] Mohd D, Fauzan F, Faizal M, et al. Energy, economic and environmental impact of wind power in Malaysia. International Journal of Advanced Scientific Research and Management 2017; 2(7): 81.

[21] Lip-Wah H, Ibrahim S, SutarjiKasmin, et al. Review of offshore wind energy assessment and siting methodologies for offshore wind energy planning in Malaysia. American International Journal of Contemporary Research 2012; 2: 72–85.

[22] Fish FE, Weber PW, Murray MM, et al. The Tubercles on Humpback Whales ' Flippers : Application of Bio-Inspired Technology. 2011; 51: 203–213.

[23] Cognet V, Courrech Du Pont S, Dobrev I, et al. Bioinspired turbine blades offer new perspectives for wind energy. Proceedings of the Royal Society A: Mathematical, Physical and Engineering Sciences 2017; 473.

[24] Lentink D, Dickson WB, Van Leeuwen JL, et al. Leading-edge vortices elevate lift of autorotating plant seeds. Science 2009; 324: 1438–1440.

[25] Minami S, Azuma A. Various flying modes of wind-dispersal seeds. Journal of Theoretical Biology 2003; 225: 1–14.

[26] Chu YJ, Chong WT. A biomimetic wind turbine inspired by Dryobalanops aromatica seed: Numerical prediction of rigid rotor blade performance with OpenFOAM®. Computers and Fluids 2017; 159: 295–315.

[27] Ikeda T, Tanaka H, Yoshimura R, et al. A robust biomimetic blade design for micro wind turbines. Renewable Energy 2018; 125: 155–165.

[28] Momeni F, Sabzpoushan S, Valizadeh R, et al. Plant leaf-mimetic smart wind turbine blades by 4D printing. Renewable Energy 2019; 130: 329–351.

[29] Seidel C, Jayaram S, Kunkel L, et al. Structural analysis of biologically inspired small wind turbine blades. International Journal of Mechanical and Materials Engineering 2017;12:1-9.

[30] Herrera C, Correa M, Villada V, et al. Structural design and manufacturing process of a low scale bio-inspired wind turbine blades. Composite Structures 2019; 208: 1–12.

[31] Elkhoury M, Kiwata T, Nagao K, et al. Wind tunnel experiments and Delayed Detached Eddy Simulation of a three-bladed micro vertical axis wind turbine. Renewable Energy 2018; 129: 63–74.

[32] Marten D, Lennie M, Pechlivanoglou G, et al. Implementation, Optimization and Validation of a Nonlinear Lifting Line Free Vortex Wake Module Within the Wind Turbine Simulation Code QBlade. Volume 9: Oil and Gas Applications; Supercritical CO2 Power Cycles; Wind Energy 2015; V009T46A019.

[33] Li C, Xiao Y, Xu Y lin, et al. Optimization of blade pitch in H-rotor vertical axis wind turbines through computational fluid dynamics simulations. Applied Energy 2018; 212: 1107–1125.

[34] Subramanian A, Yogesh SA, Sivanandan H, et al. Effect of airfoil and solidity on performance of small scale vertical axis wind turbine using three dimensional CFD model. Energy 2017; 133: 179–190.

[35]   Lee YT, Lim HC. Numerical study of the aerodynamic performance of a 500W Darrieus-type vertical-axis wind turbine. Renewable Energy 2015; 83: 407–415.

[36]   Tahani M, Rabbani A, Kasaeian A, et al. Design and numerical investigation of Savonius wind turbine with discharge flow directing capability. Energy 2017; 130: 327–338.

[37]   Hameed MS. Evaluation of Aerodynamic Forces over a Vertical Axis Wind Turbine Blade through CFD analysis. Journal of Applied Mechanical Engineering 2013; 02: 1–5.

[38]   Menni Y, Azzi A, Chamkha AJ. Optimal thermo aerodynamic performance of s-shaped baffled channels. Journal of Mechanical and Engineering Sciences 2018; 12: 3888–3913.

[39]   Sellami T, Jelassi S, Berriri H, et al. Finite volume free vibration analysis of a new aerodynamic styling wind turbine. Wind Engineering 2018; 42: 397–410.

[40]   Sayed MA, Kandil HA, Shaltot A. Aerodynamic analysis of different wind-turbine-blade profiles using finite-volume method. Energy Conversion and Management 2012; 64:541-550.

[41]   Siddiqui M, Fonn E, Kvamsdal T, et al. Finite-volume high-fidelity simulation combined with finite-element-based reduced-order modeling of incompressible flow problems. Energies 2019; 12: 1271.

[42]   Tan J. Simulation of morphing blades for vertical axis wind turbines. Concordia University, 2017.

[43]   Wang S, Bell JR, Burton D, et al. The performance of different turbulence models (URANS, SAS and DES) for predicting high-speed train slipstream. Journal of Wind Engineering and Industrial Aerodynamics 2017; 165: 46–57.

[44]   Wolfe WP. CFD Calculations of S809 Aerodynamic Characteristics. 1997; 85000.

[45]   Menter FR. Two-Equation Eddy-Viscosity Turbulence Models for Engineering Applications. 32.

[46]   Ntinas GK, Shen X, Wang Y, et al. Evaluation of CFD turbulence models for simulating external airflow around varied building roof with wind tunnel experiment. Building Simulation 2018; 11: 115–123.

[47]   Ramponi R, Blocken B. CFD simulation of cross-ventilation flow for different isolated building configurations: Validation with wind tunnel measurements and analysis of physical and numerical diffusion effects. Journal of Wind Engineering and Industrial Aerodynamics 2012; 104–106: 408–418.

[48]   Halim MAA, Mohd NARN, Nasir MNM, et al. The evaluation of k-ε and k-ω turbulence models in modelling flows and performance of s-shaped diffuser. International Journal of Automotive and Mechanical Engineering; 15.

[49]   Nobile R, Vahdati M, Barlow JF, et al. Unsteady flow simulation of a vertical axis augmented wind turbine: A two-dimensional study. Journal of Wind Engineering and Industrial Aerodynamics 2014; 125: 168–179.

[50]   Singh NK. Simulation of flow over a rotationally oscillating square cylinder at low Reynolds numbers. International Journal of Automotive and Mechanical Engineering; 16.

[51]   ANSYS Inc. ANSYS Fluent user's guide release 15.0. Knowledge Creation Diffusion Utilization 2013; 15317: 724–746.

[52]   Tian W, Song B, Van Zwieten JH, et al. Computational fluid dynamics prediction of a modified savonius wind turbine with novel blade shapes. Energies 2015; 8: 7915–7929.

[53]   Wenlong T, Baowei S, Zhaoyong M. Conceptual design and numerical simulations of a vertical axis water turbine used for underwater mooring platforms. International Journal of Naval Architecture and Ocean Engineering 2015; 5: 625–634.

[54]   Schubel PJ, Crossley RJ. Wind turbine blade design. Energies 2012; 5: 3425–3449.

[55]   Rezaeiha A, Kalkman I, Blocken B. CFD simulation of a vertical axis wind turbine operating at a moderate tip speed ratio: Guidelines for minimum domain size and azimuthal increment. Renewable Energy 2017; 107: 373–385.

[56]   Qin N, Howell R, Durrani N, et al. Unsteady Flow Simulation and Dynamic Stall Behaviour of Vertical Axis Wind Turbine Blades. Wind Engineering 2011; 35: 511–527.